Asian Journal of Chemistry; Vol. 37, No. 8 (2025), 2002-2008

ASIAN JOURNAL OF CHEMISTRY

https://doi.org/10.14233/ajchem.2025.34055

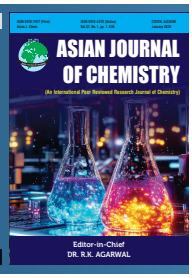

Biosynthesis of Selenium Nanoparticles utilizing Leaf Extract of *Wedelia glauca (Ortega) O. Hoffm Ex Hicken* (Asteraceae): Characterization and Evaluation of Anticancer Properties

M. SHANTHAMANI[1,*], K. KARTHIK[2], L. KRISHNAVIGNESH[3] and ANBALAGAN SRINIVASAN[1]

[1]Department of Chemistry, Government Arts College (Autonomous), Coimbatore-641018, India
[2]Department of Chemistry, School of Foundational Sciences, Kumaraguru College of Technology, Coimbatore-641049, India
[3]Department of Academics and Research, Chennai Fertility Centre and Research Institute, Chennai-600030, India

*Corresponding author: E-mail: shanthache@gmail.com

Received: 16 May 2025; *Accepted*: 16 July 2025; *Published online*: 31 July 2025; AJC-22079

This study focuses on the synthesis and biological evaluation of selenium nanoparticles (SeNPs) derived from the leaf extract of *Wedelia glauca (Ortega) O. Hoffm. Ex Hicken (Asteraceae)* through a green bioreduction process using sodium selenite. The synthesized nanoparticles were separated from the reaction mixture using high-speed centrifugation and subsequently characterized using X-ray diffraction (XRD), transmission electron microscopy (TEM) and UV-visible spectroscopy. The XRD results revealed that the SeNPs possessed a crystalline structure, with an average particle size of 21.73 nm, corroborated by TEM analysis. The SeNPs demonstrated the ability to activate immune responses against cancer cells, induce mitochondria-mediated apoptosis and exhibit significant anticancer activity both *in vitro* and *in vivo*, particularly against prostate malignancies. These findings suggest that SeNPs synthesized *via* a sustainable method hold considerable promise for biomedical and therapeutic applications.

Keywords: Asteraceae, *Wedelia glauca*, Selenium nanoparticles, Anticancer activity.

INTRODUCTION

In the field of nanomedicine, nanoparticles play a pivotal role, serving as essential tools for diagnostic applications and drug delivery systems. Their efficient production, coupled with the ability to interact synergistically with various biological components, significantly enhances their functional properties and biological efficacy [1]. Nanoparticles exhibit exceptional chemical and physical properties, which are largely attributed to their high surface area-to-volume ratio and distinct electronic characteristics. These attributes enable them to act as reactants in catalytic reactions [2]. Despite their potential, challenges such as toxicity, as well as the time and financial demands of large-scale production, remain significant barriers to practical applications [3]. Among the various nanosystems explored for biosensor development [4], selenium nanoparticles (SeNPs) have gained considerable attention due to their ability to bridge biological recognition processes with signal transduction. SeNPs are particularly appealing in developing countries owing to their low environmental toxicity [5], biocompatibility [6], conductivity [7] and electrocatalytic properties [8].

Currently, no documented studies have explored the biogenic synthesis of selenium nanoparticles (SeNPs) using the widely available and commercially accessible *Wedelia glauca (Ortega) O. Hoffm. Ex Hicken* (Asteraceae) as a biomaterial. This plant is renowned for its significant therapeutic potential in addressing various conditions, including cancer, wound healing, inflammation, central nervous system disorders and ulcers [9,10]. Additionally, *Wedelia glauca* is well-recognized for its antioxidant and antimicrobial properties, attributed to the presence of bioactive compounds such as triterpenoids and flavonoids [11,12]. Ongoing research aims to further investigate the applications of these constituents. In this context, the present study focuses on the synthesis and characterization of selenium nanoparticles (SeNPs) derived from *Wedelia glauca* and evaluates their antioxidant and *in vitro* cytotoxic properties.

EXPERIMENTAL

Synthesis of SeNPs: A plant-mediated green synthesis method was employed to produce SeNPs utilizing *Wedelia glauca* leaf extract as reducing agents. Initially, 50 mL of leaf extract was placed on a magnetic stirrer and stirred for 30 min. Separately, 0.8647 g of sodium selenite ($Na_2Se_2O_3$) was dissolved in distilled water to prepare a 50 mL solution, which was added dropwise to the stirred leaf extract a noticeable colour changes were observed, indica-ting the formation of selenium nanoparticles. The reaction mixt-ure was then centrifuged at 4500 rpm for 10 min to separate the nanoparticles. The supernatant was discarded and the resulting pellet, containing the SeNP precipitate, was rinsed with distilled water to remove any impurities. The purified pellet was dried at 70-80 ºC and then the dried powder was then collected and stored for subsequent characterization.

Characterization: The synthesized SeNPs were characterized using multiple analytical techniques. The crude extracts were analyzed using an ultraviolet-visible (Cary 8454 UV-Vis) spectrophotometer, scanning the wavelength range of 200-800 nm to identify surface plasmon resonance. FTIR spectroscopy was employed to identify the functional groups present in the plant extract that contributed to the reduction and stabilization of SeNPs. The morphology and elemental composition of the synthesized SeNPs were examined using field emission scanning electron microscopy (FE-SEM) and high-resolution transmission electron microscopy (HR-TEM) with a TECNAI G2 F30 instrument. X-ray diffraction (XRD) analysis was performed to determine the crystalline structure and average particle size of the SeNPs, further corroborating the structural data obtained from HR-TEM.

All chemicals were procured from Sigma-Aldrich Chemicals Pvt. Ltd. (India), ensuring high-grade quality suitable for biological studies. Other analytical-grade chemicals were purchased from HiMedia Laboratories Pvt. Ltd., India. The reagents and chemicals required for the biological evaluation of SeNPs included Dulbecco's modified Eagle's medium (DMEM), streptomycin, penicillin-G, L-glutamine, phosphate-buffered saline (PBS), 3-(4,5-di-methylthiazol-2-yl)-2,5-diphenyltetrazolium bromide (MTT), 2′,7′-dichlorodihydrofluorescein diacetate (DCFH-DA), sodium dodecyl sulfate (SDS), trypan blue, trypsin-EDTA and ethylene-diaminetetraacetic acid (EDTA). Additional chemicals, including acridine orange, rhodamine-123, ethidium bromide, Triton X-100, ethanol, dimethyl sulfoxide (DMSO) and bovine serum albumin (BSA), were also utilized in the assays.

Cell culture: Lung cancer (A549) cell lines were obtained from the Cell Repository of the National Centre for Cell Sciences (NCCS), Pune, India. The cells were cultured in Dulbecco's modified Eagle medium (DMEM), supplemented with 10% fetal bovine serum (FBS) to support cell growth. To prevent bacterial contamination, the medium was further supplemented with penicillin (100 U/mL) and streptomycin (100 µg/mL). The cell culture was maintained in a humidified incubator at 37 ºC with 5% CO_2 to ensure optimal growth conditions. Cell viability was assessed using the MTT assay, where 3-(4,5-dimethylthiazol-2-yl)-2,5-diphenyltetrazolium bromide (MTT) is reduced by the mitochondrial dehydrogenase of viable cells, yielding a purple formazan product. The NAD(P)H-dependent reductase in viable cells reduces MTT to formazan, resulting in a deep purple colour. The formazan crystals were then solubilized with a solubilizing solution and absorbance was measured at 500-600 nm using a plate reader.

$$\text{Inhibitory of cell proliferation (\%)} = \frac{\text{Mean absorbance of the sample}}{\text{Mean absorbance of the control}} \times 100$$

The IC_{50} value, representing the concentration required to inhibit 50% of cell proliferation, was determined from the dose-response curve, with a comparison to control cells. All experiments were performed in triplicate, with at least three independent trials to ensure reproducibility [13].

RESULTS AND DISCUSSION

The reaction mixture underwent a significant colour change after being subjected to microwaving for 20 min, indicating the successful reduction of $NaHSeO_3$ and the formation of selenium nanoparticles (SeNPs). Initially colourless, $NaHSeO_3$ turned brown upon the addition of *W. glauca* extract. These colour changes are characteristic of the formation of colloidal SeNPs and they provide visual confirmation of the reduction process. This observation supports the initial hypothesis that selenium oxyanions (SeO_3^{2-}) are reduced to elemental selenium (Se^0) through the action of polyphenols in the *W. glauca* extract [14]. The synthesized SeNPs was stored in a refrigerator for further use and no agglomeration were observed, ensuring the stability of the nanoparticles in solution over time.

FTIR spectroscopy: FTIR spectroscopy was employed to identify the functional groups present in the colloidal form of SeNPs. A broad peak observed at 3350 cm^{-1} corresponds to the O-H stretch of alcohols and phenols, while the absorption peak at 2923 cm^{-1} is attributed to the C-H stretching of alkynes (Fig. 1). The band at 1562 cm^{-1} is due to the asymmetric stretch of N-O in nitro compounds. A strong band at 1401 cm^{-1} corresponds to C-C stretching (in aromatic rings) and the sharp peak at 1345 cm^{-1} is assigned to the C-H bending in alkanes. The peak at 1001 cm^{-1} corresponds to C-N stretching in amines

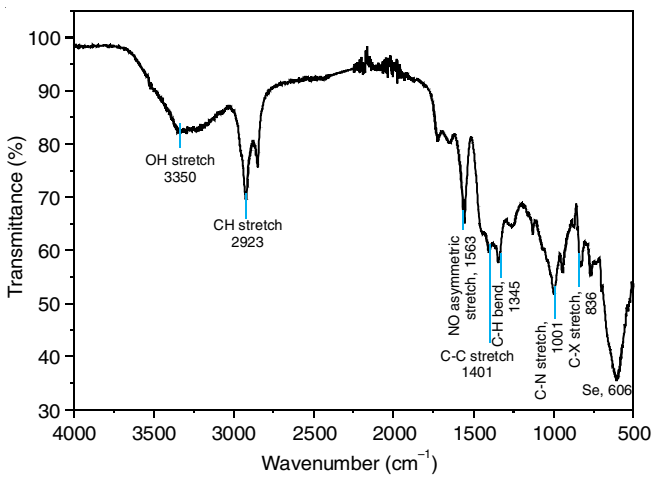

Fig. 1. FTIR spectrum of synthesized selenium nanoparticles (SeNPs)

and the band at 836 cm^{-1} is attributed to C-X stretching in alkyl halides. Furthermore, a broad and sharp peak at 606 cm^{-1} corresponds to the Se (selenium) stretching in the IR spectrum [15]. It is important to observe that reactivity increases with decreasing particle size, which can lead to nanoparticle aggregation. To prevent this, SeNPs were stabilized using various capping agents, which are present in the extract of *W. glauca*.

UV spectroscopy: The UV-Vis spectroscopy was employed to determine the surface plasmon resonance (SPR) of the SeNPs in solution. The UV-Vis spectrum of the synthesized SeNPs, shown in Fig. 2, exhibited a maximum absorption peak at 650 nm [16]. This absorbance peak is associated with the crystallizable nature of the SeNPs.

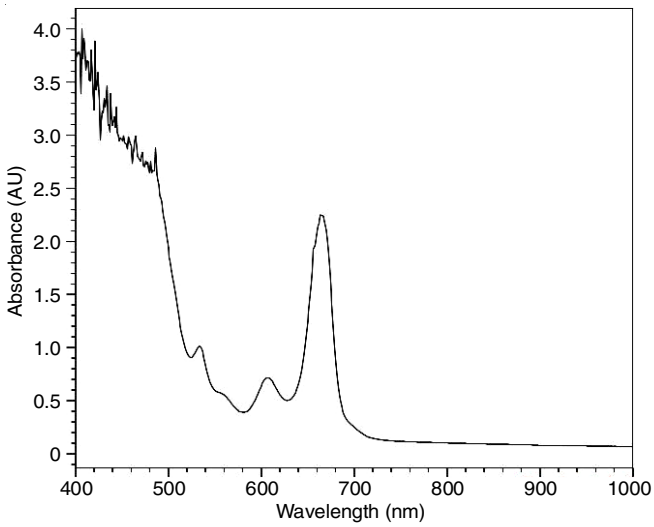

Fig. 2. UV spectrum of synthesized selenium nanoparticles (SeNPs)

Powder XRD: As shown in Fig. 3, the diffraction peaks and their corresponding planes (2θ) confirm the hexagonal crystal structure of SeNPs, matching the data in ICDD card No. 00-042-1425 [13,17]. The most intense peak observed at 29.70º (101) indicates the major orientation of the SeNPs along the (101) plane and suggests high purity in the green-synthesized SeNPs. The crystallite size was calculated from

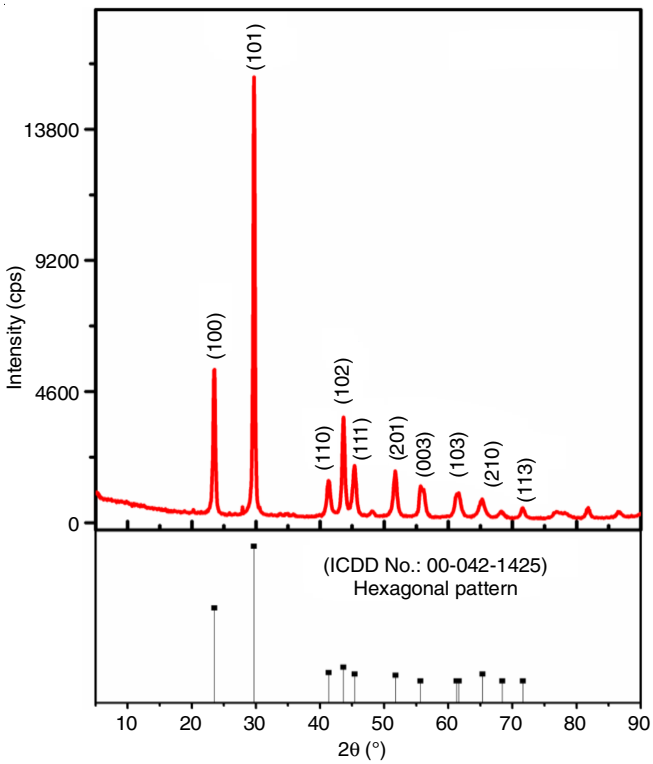

Fig. 3. Powder XRD pattern of green synthesized SeNPs (obtained crystal pattern matched with std. ICCD database)

the full width at half maximum (FWHM) of the (101) peak using the Debye-Scherrer equation (eqn. 1) [18,19].

$$D = \frac{K\lambda}{\beta\cos\theta}$$

where D = crystallite size, K = Scherer constant (0.9), λ = wavelength of X-ray (1.54 nm), β = FWHM of Bragg's angle. The calculated crystallite particle size is around 32.93 nm and it could be stated that SeNPs were crystallized as hexagonal symmetry with lattice parameters around a = 4.3580 (Å), b = 4.3580 (Å) and c = 4.9500 (Å) (Table-1).

Morphological studies: Scanning electron microscopy (SEM) was used to investigate the morphology of selenium

TABLE-1
DIFFRACTION PEAKS AND THEIR CORRESPONDING PLANES

2θ values (º)		d-spacing	Miller indices (d_{hkl}) Assigned	Crystallographic parameters (selenium)
Experimental	Standard (ICDD:00-042-1425)			
23.50074	23.529	3.77800	(100)	
29.70771	29.726	3.00300	(101)	
41.37583	41.365	2.18100	(110)	
43.65247	43.671	2.07100	(102)	
45.36254	45.402	1.99600	(111)	Crystal system: Hexagonal Space group: P3121 Space group number: 152 a (Å) = 4.3580 b (Å) = 4.3580 c (Å) = 4.9500
48.13453	–			
51.72210	51.784	1.76400	(201)	
55.56001	55.697	1.64900	(003)	
56.21218	–			
61.20863	61.300	1.51100	(103)	
–	61.662			
65.27463	65.341	1.42700	(210)	
68.27115	68.425	1.37000	(211)	
71.57467	71.653	1.31600	(113)	

nanoparticles (SeNPs) synthesized *via* a green method using *Wedelia glauca* leaf aqueous extract. Fig. 4 presents the FE-SEM image, revealing a predominant presence of defective, highly fragmented nano-cylindrical rods and platelets. These morphological features suggest potential applications in catalytic processes. It is hypothesized that nanoparticle aggregation dominates the reduction process and the primary nucleation of reduced selenium atoms. This aggregation may be due to the extensive number of functional groups in the *W. glauca* leaf extract, which interact with and nucleate selenious acid ions. The more accessible metal ions appear to be involved in fewer nucleation events, leading to the agglomeration of nanoparticles [20]. Previous studies have reported that aggregated nanoparticles tend to exhibit enhanced biological activity [21,22]. Thus, the *W. glauca* extract-mediated SeNPs may offer promising pharmacological applications.

Transmission electron microscopy (TEM) analysis of the green-synthesized SeNPs revealed the formation of paddy-like structures, with an average particle size of approximately 350 nm (Fig. 5a-c). High-resolution TEM (HR-TEM) images

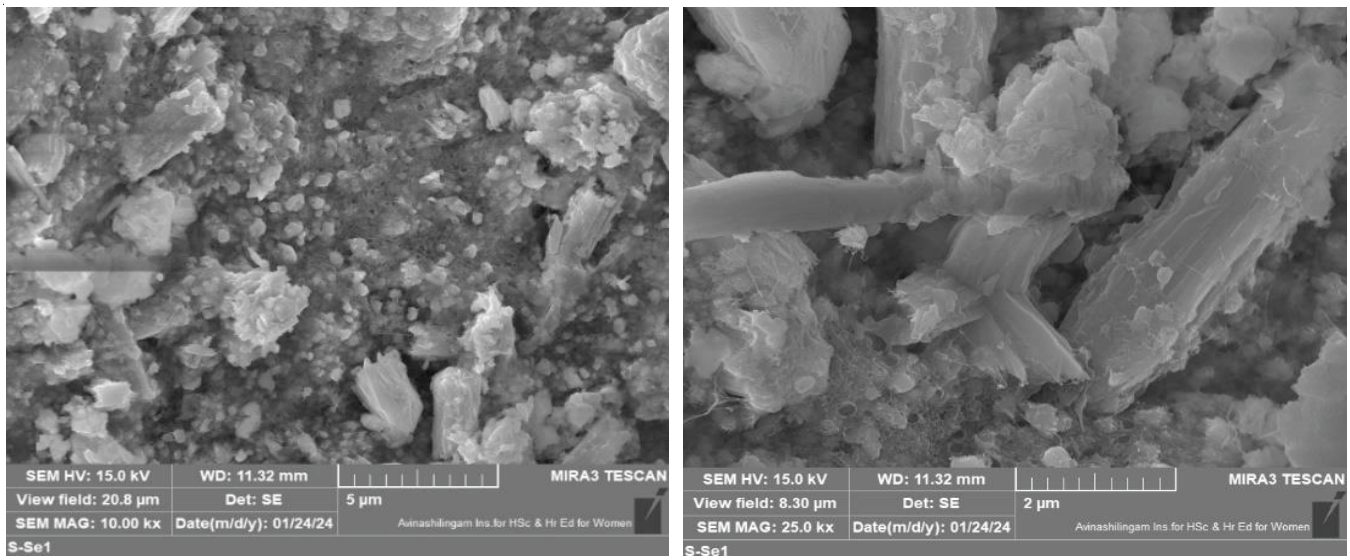

Fig. 4. SEM images of green synthesized Se NPs (obtained highly broken nano cylindrical rods and platelets)

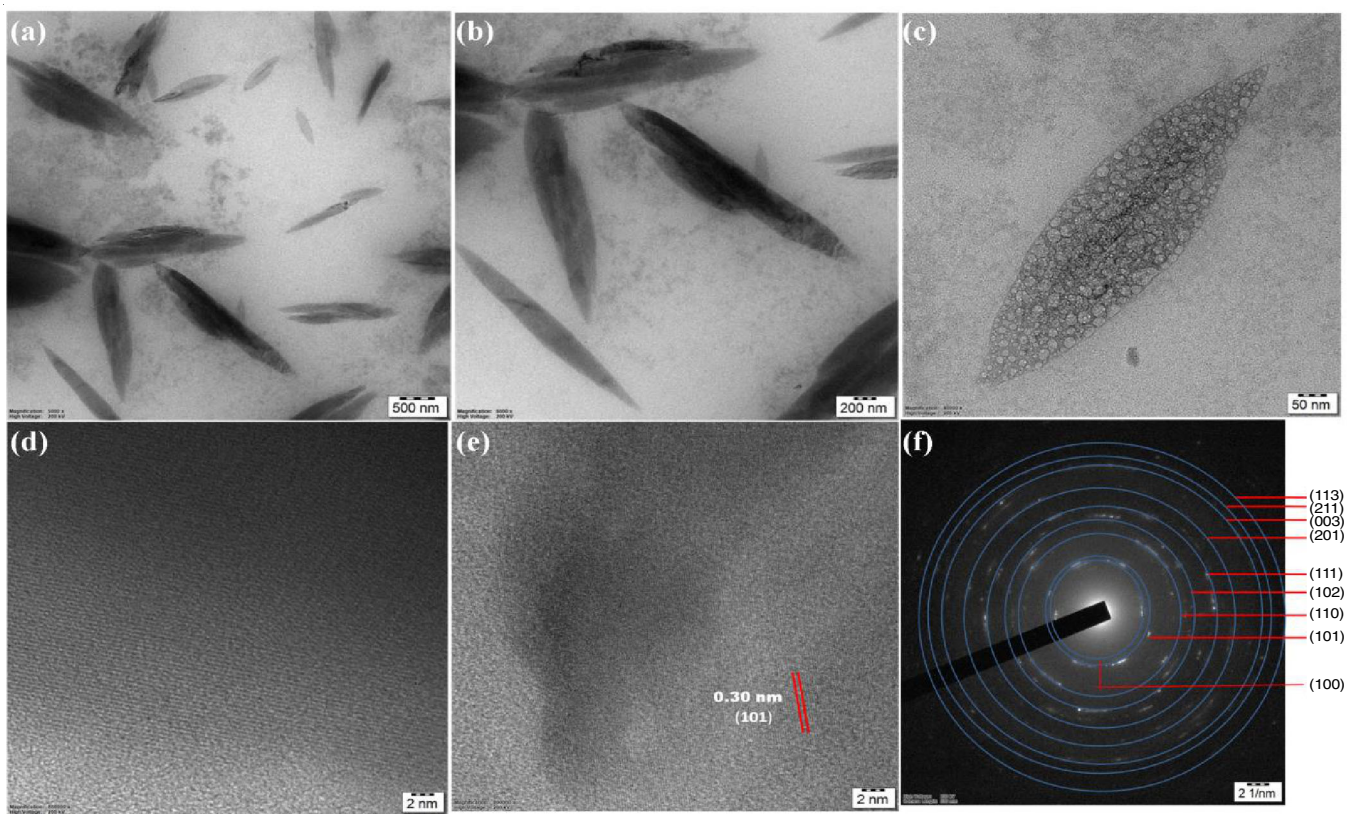

Fig. 5. TEM images (a-c), HR-TEM images with fringes (d, e) and SAED patterns of green synthesized SeNPs

further revealed the d-spacing value, which was calculated to be 0.3 nm, perfectly matching the (101) plane. This plane corresponded to the most intense peak observed in the powder X-ray diffraction (P-XRD) analysis, confirming consistency between the TEM and P-XRD data. The SAED pattern of the synthesized SeNPs indicated their crystalline nature [23,24]. The diffraction rings corresponded to the planar reflections of the (100), (101), (110) and (102) planes of crystalline selenium (Fig. 5e). These results are consistent with the recent reports demonstrating the biosynthesis of SeNPs using *W. glauca* leaf extract [25].

Biological activity: Photomicrograph (20x) represents morphological changes in A549 cells such as shrinkage, detachment, membrane blebbing and distorted shape induced by sample S-Se3 treatment (15 and 20 µg/mL for 24 h) as compared with control. Control showed normal intact cell morphology and their images were captured by light microscope. The biological activity of the synthesized selenium nanoparticles (S-Se3) was evaluated by measuring the optical density (OD) values at varying concentrations and comparing the results to the control group. The OD values were recorded for three replicates at each concentration of the sample and the corresponding percentage of cell viability was calculated.

Optical density (OD) measurements: The OD values of the control and treated samples at different concentrations (2.5, 5, 7.5, 10, 15 and 20 µg) are shown in Table-2. The control group exhibited the highest OD value, indicating normal cell viability, with a mean value of approximately 0.1927. In contrast, the OD values of the treated samples gradually decreased with increasing concentrations of the S-Se3 sample, suggesting a dose-dependent inhibition of cell viability. At 2.5 µg concentration, the OD values ranged from 0.179 to 0.198, reflecting a slight reduction in cell viability. As the concentration of S-Se3 increased to 5 µg, 7.5 µg and beyond, the OD values continued to decrease, with the lowest values observed at the highest concentration of 20 µg (OD = 0.048 to 0.042). These reductions in OD values are indicative of the increasing cytotoxic effects of SeNPs, suggesting a strong dose-dependent response.

Percentage of cell viability: The cell viability was calculated as a percentage relative to the control group. At the lowest concentration (2.5 µg), the viability ranged from 89.27% to 94.46% exibhiting the minimal inhibition. However, as the concentration of S-Se3 increased, there was a clear reduction in cell viability. At 5 µg, the viability ranged from 78.89% to 83.56% and at 7.5 µg, the viability dropped to approximately 71.63% to 82.00%. At concentrations of 10 µg, 15 µg and 20 µg, the cell viability significantly decreased, with the lowest values observed at 20 µg (cell viability: 24.91% to 23.88%). This indicates that higher concentrations of S-Se3 caused more substantial inhibition of cell growth, leading to a reduction in cell survival.

IC_{50} calculation: Based on data, the IC_{50} value for S-Se3 was calculated to be approximately 11.78 µg/mL, confirmed the effective cytotoxicity of the green synthesized SeNPs at lower concentrations. The observed dose-dependent reduction in cell viability strongly suggests that SeNPs synthesized from *W. glauca* possess significant cytotoxic properties. The data also demonstrates that as the concentration of S-Se3 increases, the nanoparticles exert a more pronounced inhibitory effect on cancer cell proliferation. The low IC_{50} value further highlights the potency of SeNPs in inhibiting cell growth, which is a promising characteristic for their potential use in cancer therapy.

Cell viability of S-Se3 sample on A549 lung cancer cell line using MTT assay: The cytotoxic effects of the synthesized selenium nanoparticles (S-Se3) on A549 lung cancer cells were assessed using the MTT assay. Table-3 indicates a clear dose-dependent decrease in cell viability as the concentration of S-Se3 increased. In control group, which represents untreated A549 cells, the cell viability remained at 100%, showing no cytotoxic effect from the culture medium or the experimental conditions. At a concentration of 2.5 µg/mL, the cell viability remained relatively high, with values ranging from 89.27% to 94.46%, yielding an average of 92.21%. This indicates that at low concentrations, the S-Se3 nanoparticles have only a minor inhibitory effect on cell viability, with minimal variation between replicates (SD = 2.66%). As the concentration of S-Se3 increased to 5 µg/mL, there was a more noticeable reduction in cell viability, ranging from 78.89% to 83.56% and an average of 81.49%. The SD value of 2.38% further confirmed that the reduction in viability is consistent across replicates. This demonstrates that S-Se3 nanoparticles begin to exert more significant cytotoxic effects as the concentration increases.

At 7.5 µg/mL, the cell viability further decreased to an average of 68.69%, with individual readings ranging from 66.95% to 71.63%. The SD value of 2.56% reflects a moderate variation, but the trend clearly shows that the inhibitory effects of S-Se3 continue to grow with increasing concentrations. At higher concentrations of 10 µg/mL, the average cell viability dropped to 46.19%, with values ranging between 44.64% and 47.75%. The SD value was relatively low at 1.56%, indicating stable results across replicates and further confirming that at

TABLE-2
OPTICAL DENSITY VALUES OF S-Se3

Control	2.5 µg	5 µg	7.5 µg	10 µg	15 µg	20 µg
W2	W3	W4	W5	W6	W7	W8
0.192	0.179	0.152	0.138	0.089	0.067	0.048
0.188	0.182	0.161	0.130	0.092	0.058	0.042
0.198	0.172	0.158	0.129	0.086	0.060	0.046
0.192667						
	92.90641	78.89260	71.62617	46.19369	34.77503	24.91345
	94.46350	83.56387	67.47393	47.75078	30.10375	21.79927
	89.27320	82.00678	66.95490	44.63660	31.14181	23.87539

TABLE-3
CELL VIABILITY OF SAMPLE (S-SE3) BY LUNG CANCER A549 CELL LINE USING MTT ASSAY

Concentration (µg/mL)	Cell viability (%)			Average	SD
	R1	R2	R3		
Control	100	100	100	100	0
2.5	92.90641	94.4635	89.27320	92.21437	2.663455
5.0	78.89260	83.56387	82.00678	81.48775	2.378494
7.5	71.62617	67.47393	66.95490	68.68500	2.560314
10.0	46.19369	47.75078	44.63660	46.19369	1.557090
15.0	34.77503	30.10375	31.14181	32.00686	2.452846
20.0	24.91345	21.79927	23.87539	23.52937	1.585663

this concentration, S-Se3 nanoparticles exert a strong cytotoxic effect, resulting in significant inhibition of cell growth.

At even higher concentrations of 15 µg/mL, the cell viability decreased to an average of 32.01%, with values ranging from 30.10% to 34.78% and an SD of 2.45% (Table-3). This suggests that as the concentration of S-Se3 increases, the cytotoxic effect intensifies, leading to the substantial cells death. The most significant decrease in cell viability was observed at 20 µg/mL, where the average viability was reduced to 23.53%, with values ranging from 21.80% to 24.91%. The SD value of 1.59% indicates that the results were consistent across replicates and the substantial inhibition of cell growth at this concentration emphasizes the potent cytotoxicity of SeNPs. These results indicate that the synthesized SeNPs exhibit potent cytotoxic effects in a dose-dependent manner against A549 lung cancer cells. The significant reduction in cell viability, particularly at concentrations of 10 µg/mL and above, highlights the effectiveness of S-Se3 as an anticancer agent. The calculated IC_{50} value, which corresponds to the concentration needed to inhibit 50% of cell viability, is likely between 10 µg/mL and 15 µg/mL, further supporting the efficacy of SeNPs in targeting cancer cells. These findings underscore the potential therapeutic applications of SeNPs in cancer treatment, especially for lung cancer, where they may serve as an effective agent to inhibit cancer cell proliferation.

The cytotoxicity of the synthesized SeNPs (S-Se3) on the A549 lung cancer cell line was evaluated using the MTT assay. The results presented as cell viability percentages, demonstrated a dose-dependent reduction in cell viability as the concentration of S-Se3 increased. In the control group, which represents untreated A549 cells, the cell viability was 100%, indicating no cytotoxic effect from the experimental conditions. At a concentration of 2.5 µg/mL, the cell viability decreased slightly to 92.21%, with a standard deviation (SD) of 2.66%. This indicates that at lower concentrations, the SeNPs exert a minimal cytotoxic effect. As the concentration increased to 5 µg/mL, the cell viability further reduced to 81.49%, with SD of 2.38%, signifying a more pronounced inhibition of cell growth. The trend continued with increasing concentrations at 7.5 µg/mL, the cell viability further decreased to 68.69%, showing a more substantial cytotoxic effect. The SD at this concentration was 2.56%, indicating moderate variation in the results. At higher concentrations of 10 µg/mL, the cell viability was reduced to 46.19%, with an SD of 1.56%, reflecting a consistent and significant reduction in cell viability. The decrease in viability continued at 15 µg/mL, where the cell viability reached 32.01% with an SD of 2.45%, indicating that the nanoparticles exert a strong dose-dependent cytotoxic effect on the A549 cells. At the highest concentration of 20 µg/mL, the cell viability was reduced to 23.53%, with an SD of 1.59%. The results clearly show that the SeNPs exhibit dose-dependent cytotoxicity, with a substantial decrease in cell viability as the concentration of S-Se3 increases.

Conclusion

In this study, selenium nanoparticles (SeNPs) were successfully synthesized using the leaves of *Wedelia glauca*, a locally abundant and cost-effective plant. The green synthesis process, which is straightforward, economical and eco-friendly, involved the extraction of the plant's active components, followed by their interaction with a diluted sodium selenite solution, resulting in the formation of SeNPs. The synthesized SeNPs were characterized using UV-Vis spectroscopy, FTIR, SEM, EDX and TEM techniques. The UV-Vis spectrum indicated the successful formation of SeNPs, with a characteristic absorption peak at 650 nm. FTIR analysis confirmed the presence of functional groups from the plant extract involved in reducing and stabilizing the nanoparticles. SEM and TEM analysis revealed the morphology of the SeNPs, showing paddy like structures and a crystalline nature, with an average particle size of around 21.73 nm, as confirmed by XRD analysis. EDX further validated the presence of selenium in the nanoparticles. The SeNPs exhibited significant cytotoxicity in a dose-dependent manner, with a calculated IC_{50} value between 10-15 µg/mL. At the highest concentration of 20 µg/mL, the cell viability was reduced to approximately 23.53%, confirming the potent anticancer potential of the SeNPs.

CONFLICT OF INTEREST

The authors declare that there is no conflict of interests regarding the publication of this article.

REFERENCES

1. M.A. Khudier, H.A. Hammadi, H. Al-Karagoly, S. Albukhaty, H.T. Atyia, G.M. Sulaiman, Y.H. Dewir and H.B. Mahood, *Cogent Food Agric.*, **9**, 2245612 (2023); https://doi.org/10.1080/23311932.2023.2245612
2. R.K.A. Amali, H.N. Lim, I. Ibrahim, N.M. Huang, Z. Zainal and S.A.A. Ahmad, *Trends Environ. Anal. Chem.*, **31**, e00135 (2021); https://doi.org/10.1016/j.teac.2021.e00135

3. L. Xuan, Z. Ju, M. Skonieczna, P.-K. Zhou and R. Huang, *MedComm.*, **4**, e327 (2020); https://doi.org/10.1002/mco2.327
4. M. Laad and B. Ghule, *Groundw. Sustain. Dev.*, **20**, 100888 (2023); https://doi.org/10.1016/j.gsd.2022.100888
5. K. Badgar and J. Prokisch, *Open J. Anim. Sci.*, **11**, 532 (2021); https://doi.org/10.4236/ojas.2021.114036
6. M. Khatun, Z. Khatun, M.R. Karim, M.R. Habib, M.H. Rahman and M.A. Aziz, *Food Chem. Adv.*, **3**, 100386 (2023); https://doi.org/10.1016/j.focha.2023.100386
7. K. Kalishwaralal, S. Jeyabharathi, K. Sundar, S. Selvamani, M. Prasanna and A. Muthukumaran, *Mater. Sci. Eng. C*, **92**, 151 (2018); https://doi.org/10.1016/j.msec.2018.06.036
8. A. Hussain, M.N. Lakhan, A. Hanan, I.A. Soomro, M. Ahmed, F. Bibi and I. Zehra, *Mater. Today Sustain.*, **23**, 100420 (2023); https://doi.org/10.1016/j.mtsust.2023.100420
9. S. Ruffinengo, M. Eguaras, I. Floris, C. Faverin, P. Bailac and M. Ponzi, *J. Econ. Entomol.*, **98**, 651 (2005); https://doi.org/10.1603/0022-0493-98.3.651
10. M.T. Sobrero, M. del C. Ochoa and S. Chaila, *Planta daninha*, **22**, 71 (2004); https://doi.org/10.1590/S0100-83582004000100009
11. J.C. Oberti, A.B. Pomilio and E.G. Gros, *Phytochemistry*, **19**, 2501 (1980); https://doi.org/10.1016/0031-9422(80)83044-5
12. L. Krishnavignesh and A. Mahalakshmipriya, *Int. J. Pharm Bio. Sci.*, **8**, 21 (2017); https://doi.org/10.22376/ijpbs.2017.8.4.b21-29
13. T. Mosmann, *J. Immunol. Methods*, **65**, 55 (1983); https://doi.org/10.1016/0022-1759(83)90303-4
14. S.J. Hewlings and D.S. Kalman, *Foods*, **6**, 92 (2017); https://doi.org/10.3390/foods6100092
15. F. Coccia, L. Tonucci, D. Bosco, M. Bressan and N. d'Alessandro, *Green Chem.*, **14**, 1073 (2012); https://doi.org/10.1039/c2gc16524d
16. M. Vahdati and T. Tohidi Moghadam, *Sci. Rep.*, **10**, 510 (2020); https://doi.org/10.1038/s41598-019-57333-7
17. N. Shahabadi, S. Zendehcheshm and F. Khademi, *Biotechnol. Rep.*, **30**, e00615 (2021); https://doi.org/10.1016/j.btre.2021.e00615
18. V. Sreeja, K.N. Jayaprabha and P.A. Joy, *Appl. Nanosci.*, **5**, 435 (2015); https://doi.org/10.1007/s13204-014-0335-0
19. B.A. Al Jahdaly, N.S. Al-Radadi, G.M. Eldin, A. Almahri, M. Ahmed, K. Shoueir and I. Janowska, *J. Mater. Res. Technol.*, **11**, 85 (2021); https://doi.org/10.1016/j.jmrt.2020.12.098
20. N. Jha, P. Esakkiraj, A. Annamalai, A.K. Lakra, S. Naik and V. Arul, *J. Trace Elem. Miner.*, **2**, 100019 (2022); https://doi.org/10.1016/j.jtemin.2022.100019
21. M. Sathishkumar, K. Sneha and Y.S. Yun, *Bioresour. Technol.*, **101**, 7958 (2010); https://doi.org/10.1016/j.biortech.2010.05.051
22. J.M. Zook, R.I. Maccuspie, L.E. Locascio, M.D. Halter and J. Elliott, *Nanotoxicology*, **5**, 517 (2011); https://doi.org/10.3109/17435390.2010.536615
23. C. Bantz, O. Koshkina, T. Lang, H.J. Galla, C.J. Kirkpatrick, R.H. Stauber and M. Maskos, *Beilstein J. Nanotechnol.*, **5**, 1774 (2014); https://doi.org/10.3762/bjnano.5.188
24. H. Kong, J. Yang, Y. Zhang, Y. Fang, K. Nishinari and G.O. Phillips, *Int. J. Biol. Macromol.*, **65**, 155 (2014); https://doi.org/10.1016/j.ijbiomac.2014.01.011
25. Y. Bai, Y. Wang, Y. Zhou, W. Li and W. Zheng, *Mater. Lett.*, **62**, 2311 (2008); https://doi.org/10.1016/j.matlet.2007.11.098